

# *XMM–Newton* observations of the ultra-compact binary RX J1914+24

Gavin Ramsay,<sup>1</sup>\* Pasi Hakala,<sup>2</sup> Kinwah Wu,<sup>1</sup> Mark Cropper,<sup>1</sup> K. O. Mason,<sup>1</sup>  
F. A. Córdova<sup>3</sup> and W. Priedhorsky<sup>4</sup>

<sup>1</sup>*Mullard Space Science Laboratory, University College London, Holmbury St. Mary, Dorking, Surrey, RH5 6NT*

<sup>2</sup>*Observatory, University of Helsinki, PO Box 14, FIN-00014 University of Helsinki, Finland*

<sup>3</sup>*University of California, Riverside, CA 92521, USA*

<sup>4</sup>*Los Alamos National Laboratory, MS D436, Los Alamos, NM 87545, USA*

Accepted 2004 October 31. Received 2004 October 22; in original form 2004 July 16

## ABSTRACT

We present *XMM–Newton* observations of the 569-s-period system RX J1914+24 (V407 Vul). This period is believed to represent the binary orbital period making it an ultracompact binary system. By comparing the phase of the rise to maximum X-ray flux at various epochs (this includes observations made using *ROSAT*, *ASCA* and *Chandra*) we find that the system is spinning up at a rate of  $3.17 \pm 0.07 \times 10^{-12} \text{ s s}^{-1}$ . We find that the spectra soften as the X-ray flux declines towards the off-phase of the 569-s period. Further, the spectra are best fitted by an absorbed blackbody component together with a broad emission feature around 0.59 keV. This emission feature is most prominent at the peak of the on-phase. We speculate on its origin.

**Key words:** binaries: general — stars: individual: RX J1914+24 – novae, cataclysmic variables – X-rays: stars.

## 1 INTRODUCTION

RX J1914+24 (also known as V407 Vul) is one of three sources discovered in recent years that show intensity variations on periods of less than  $\sim 10$  min. As no other periods have been detected in these systems and for other reasons, these periods have been associated with the binary orbital period. As such, these systems would have the shortest binary period of any known system. In addition, they would be amongst the strongest sources of constant gravitational radiation in the sky and easily detectable using the future *LISA* space mission. Their nature, however, remains controversial.

Of the three systems, ES Cet (Warner & Woudt 2002), with a period of 620 s, has been shown to have an accretion disc. Both RX J1914+24 (Cropper et al. 1998; Ramsay et al. 2000; Ramsay et al. 2002b) with a period of 569 s and RX J0806+15 (Israel et al. 2002; Ramsay, Hakala & Cropper 2002a) with a period of 321 s do not show evidence for an accretion disc and share many similar properties. Their X-ray light curves are almost identical, being off for around half their cycle, showing a sharp rise to maximum flux and a more gradual decay. In contrast, their optical light curves are sinusoidal in shape and in antiphase with the X-ray phase (Ramsay et al. 2000; Israel et al. 2003). The period of both systems are reported to be evolving in the same direction (i.e. spinning up) as predicted if their binary orbit is evolving through gravitational radiation (Hakala et al. 2003; Strohmayer 2003; Hakala, Ramsay & Byckling 2004 for RX J0806+15 and Strohmayer 2002, 2004a for RX J1914+24).

They do, however, differ in some respects. RX J0806+24 shows weak optical emission lines, with hydrogen blending with helium lines (Israel et al. 2002; Norton, Haswell & Wynn 2004). On the other hand, RX J1914+24 shows a generally featureless optical spectrum but with weak absorption lines that appear similar to that of a K star (Steehgs et al., in preparation). At present, it is unclear as to how to interpret this spectrum, although a triple system is a possibility.

RX J1914+24 has been observed in X-rays using *ROSAT*, *ASCA* (Cropper et al. 1998; Ramsay et al. 2000; Ramsay et al. 2002b) and *Chandra* (Strohmayer 2004a). With its larger effective area, *XMM–Newton* provides the possibility of obtaining phase resolved spectroscopy through the 569-s cycle. Here, we present observations of RX J1914+24 made using *XMM–Newton*.

## 2 OBSERVATIONS AND DATA REDUCTION

*XMM–Newton* was launched in 1999 December by the European Space Agency (ESA). The EPIC instruments contain imaging detectors covering the energy range 0.15–10 keV with moderate spectra resolution (EPIC pn, Strüder et al. 2001, EPIC MOS, Turner et al. 2001), while the RGS has a high spectral resolution between 0.3–2 keV (den Herder et al. 2001). The observation log is shown in Table 1.

The EPIC pn detector was configured in small window mode and thin filter, the EPIC MOS1 detector in timing mode and thin filter, and the EPIC MOS2 detector in small window mode and medium filter. The Optical Monitor used two UV filters (UVW2 and UVM2).

\*E-mail: gtbr@mssl.ucl.ac.uk

**Table 1.** The observation log of *XMM-Newton* observations of RX J1914+24. The start time is in UTC.

<i>XMM</i> orbit	Start date	Duration (ks)	Mean EPIC pn (count s <sup>-1</sup> )
0718	2003-11-09:22:36:10	9.5	0.80
0721	2003-11-15:22:08:26	8.5	0.73

Because of the high extinction to RX J1914+24 (Cropper et al. 1998), RX J1914+24 was not detected, as expected, in either filter.

The X-ray data were processed using the *XMM-Newton* SCIENCE ANALYSIS SOFTWARE (SAS) v6.0. The data were barycentrically corrected and in units of TERRESTRIAL TIME (TT). For the EPIC detectors (Strüder et al. 2001; Turner et al. 2001), data were extracted using an aperture of 40 arcsec centred on the source position: this is  $\sim 87$  per cent of the encircled energy. Background data were extracted from a source-free region. The background data were scaled and subtracted from the source data. We show the mean background subtracted EPIC pn count rate for the two observations in Table 1. We extracted the RGS spectra in the standard way using RGSPROC. Although they were of low signal-to-noise ratio, no bright distinct lines were detected.

### 3 LIGHT CURVES

We show the folded and binned light curve in three energy bands in Fig. 1. As found by previous X-ray studies, the system is off for  $\sim 0.4$  cycles. We extracted images of the field of RX J1914+24 during the off phase using the EPIC pn data and do not detect RX J1914+24. After the off-phase, there is a sharp increase in flux in the 0.15–0.5 (soft) and 0.5–1.0 keV (medium) bands. The softness curve (soft/medium; Fig. 1), shows that the spectrum of RX J1914+24 softens towards the descent from the peak intensity of the bright phase. This implies that the X-ray emission region has a temperature structure. We also show the 1–2 keV (hard) folded light curve in Fig. 1: the count rate is much reduced compared with the soft or medium bands. It shows a pronounced drop in intensity at the point where the softness curve starts to soften.

Ramsay et al. (2000) showed using *ASCA* data that RX J1914+24 has no significant flux above 2 keV. With the higher effective area of *XMM-Newton* compared with *ASCA*, we can test this assertion more rigorously. We extracted images of the immediate field around RX J1914+24 using data from the EPIC pn detector taken at both epochs. There is no significant detection above 2.0 keV in either epoch. To determine an upper limit to the hard X-ray emission, we added a Bremsstrahlung component to the model described in Section 5. For a temperature of  $kT = 10$  keV we find an upper limit to the 2–10 keV unabsorbed flux of  $1.3 \times 10^{-13}$  erg s<sup>-1</sup> cm<sup>-2</sup>, which reduces to  $9.6 \times 10^{-15}$  erg s<sup>-1</sup> cm<sup>-2</sup> for  $kT = 1$  keV.

We searched for periods above 20 min using all the *ROSAT*, *ASCA*, *Chandra* and *XMM-Newton* data, and just the *XMM-Newton* separately. We found no evidence for a significant period(s) in either combination of data. (Care has to be taken because the *ROSAT* data are in units of UTC; *ASCA* is on a system very close to UTC, while *Chandra* and *XMM-Newton* data are in TT).

### 4 PHASING OF THE DATA

Strohmayer (2002) performed a coherent timing analysis of *ROSAT* and *ASCA* data and found that the 569-s period in RX J1914+24 was

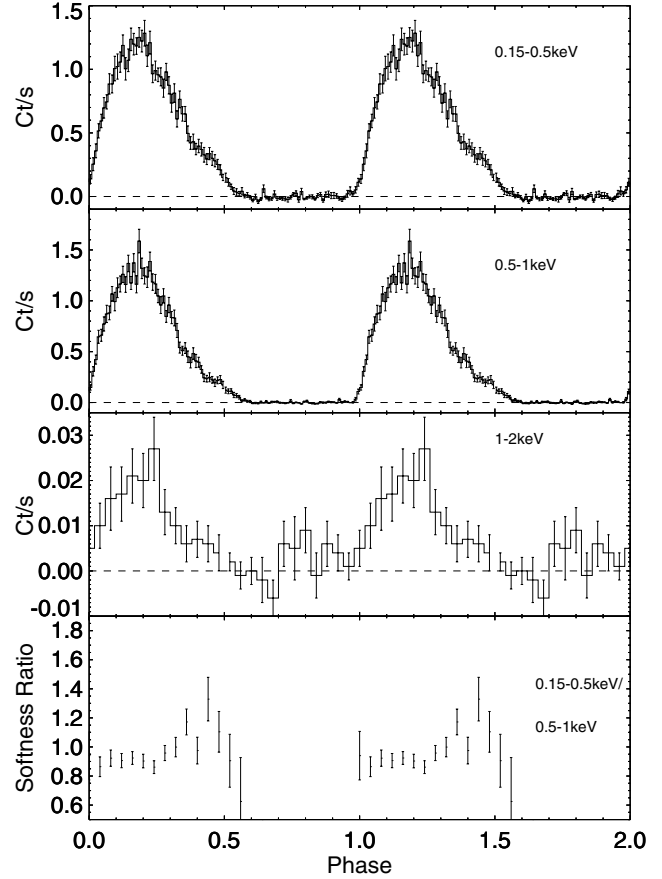


**Figure 1.** From the top: the folded and binned light curve in the 0.15–0.5, 0.5–1.0, 1–2 keV band and the softness curve (0.15–0.5/0.5–1.0 keV). The soft and medium bands are binned into 100 bins, the hard band into 25 bins and the softness ratio curve into 25 bins. The data have been folded on  $T_o = 2449258.033373137$  (BJD), and the mean period between  $T_o$  and  $T_{XMM}$  (to ensure proper phasing of the data).

spinning up at a rate of  $8 \pm 3 \times 10^{-18}$  Hz s<sup>-1</sup> ( $= 2.6 \times 10^{-12}$  s s<sup>-1</sup>). This was later refined with the addition of *Chandra* data to  $7.0 \pm 0.8 \times 10^{-18}$  Hz s<sup>-1</sup> ( $= 2.3 \times 10^{-12}$  s s<sup>-1</sup>, Strohmayer 2004a). This result was consistent with the expected spin-up rate if the systems was being driven entirely by gravitational radiation and the secondary star has a low mass.

The spin-up in both RX J0806+15 and RX J1914+24 has been met with some degree of scepticism (e.g. Woudt & Warner 2003). To show the effect of the spin-up in RX J1914+24, we show in Fig. 2 the *ROSAT*, *ASCA*, *Chandra* (which were extracted from the *Chandra* archive and reduced in the same manner as Strohmayer 2004a) and *XMM-Newton* data folded on the constant period term ( $1/\nu_0$ ) of Strohmayer (2004a). The phase of the rise to maximum flux has continued to arrive progressively earlier because of the epoch of the *Chandra* data: it is clear that RX J1914+24 is spinning up. It is highly unlikely that the true period is a side-band power peak Strohmayer (2004a).

For the phased light curves shown in Fig. 2, we estimated the start of the bright phase by noting the phase at which the count rate rose by a significant level compared with the previous phase bin. We show how the start of the bright phase varies over time in Fig. 3 together with an estimate of the uncertainty in the phase. We fitted these points with a constant  $\dot{P}$  term: the best fit is shown as a solid

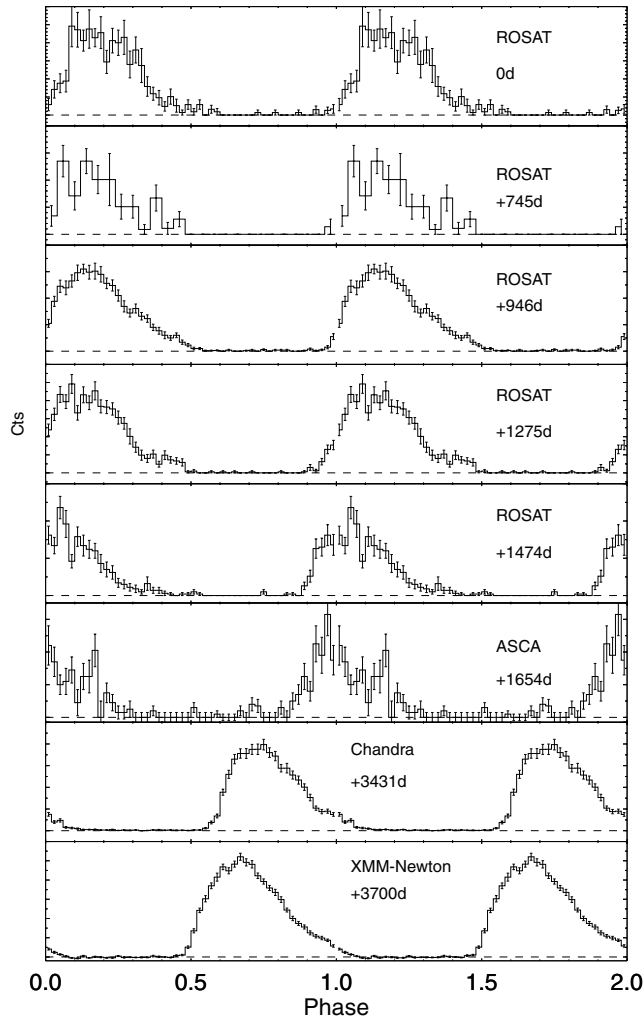


**Figure 2.** The *ROSAT*, *ASCA*, *Chandra* and *XMM–Newton* data folded on the best-fitting period of Strohmayer (2004a). It shows the phase at which the rise to maximum in X-rays occurs earlier over time: i.e. it is spinning up.

line in Fig. 2. We note that the shift in phase for a constant  $\dot{P}$  term is not linear over time (see Cropper et al. 2004). We find a spin-up rate of  $3.17 \pm 0.10 \times 10^{-12} \text{ s s}^{-1}$  ( $=1.0 \times 10^{-17} \text{ Hz s}^{-1}$ ). Because the errors on the phase of the rise to the bright phase are not strictly  $1\sigma$  errors, we determined the error using a bootstrap method. This gave a larger error than the formal error to the fit ( $0.07 \times 10^{-12} \text{ s s}^{-1}$ ). The spin-up rate that we determine is slightly greater than the spin-up rate derived by Strohmayer (2004a).

We also show the long-term X-ray intensity of RX J1914+24 in the lower panel of Fig. 3. These values were obtained by converting the peak X-ray count rate in each epoch to the equivalent *ROSAT* High Resolution Imager (HRI) count rate (because most observations were determined using this instrument). We used the spectral parameters shown in Table 2 and the *PIMMS* tool (Mukai 1993) to convert the count rate in other detectors to that expected for the *ROSAT* HRI. We note that the largest residual to the fit occurred after the peak X-ray flux had decreased from a short epoch of enhanced X-ray emission. However, the deviation is small ( $1.9\sigma$ ), so therefore probably not significant.

Ramsay et al. (2000) showed that the peak of the X-ray and optical band emission were offset in phase. Because their *ASCA* and *I*-band

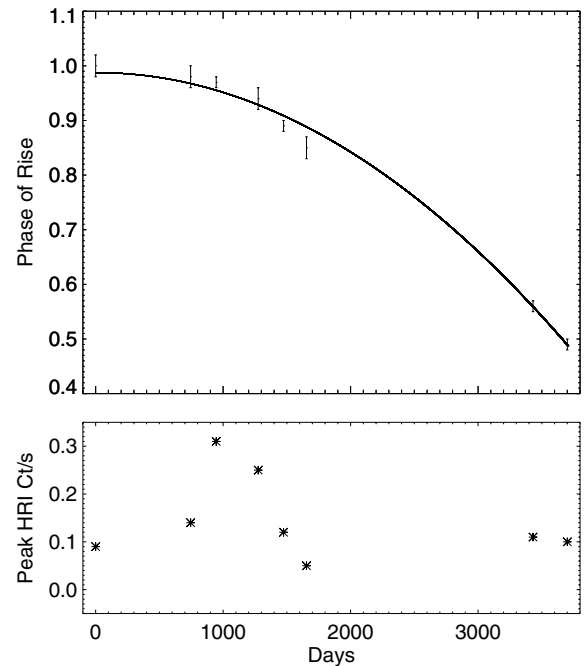


**Figure 3.** Top panel: the phase of the sharp rise to maximum X-ray flux determined for all the epochs shown in Fig. 2 determined using a constant period,  $P_o$ . The solid line shows the best fit to the data giving a spin-up rate of  $3.17 \times 10^{-12} \text{ s s}^{-1}$ . Lower panel: the X-ray intensity of the peak of the bright phase expressed in equivalent *ROSAT* HRI count  $\text{s}^{-1}$ . The start date is JD = 2449259. We show the error on the phase of the sharp rise, while the error on the X-ray intensity is smaller than the plotted symbol.

**Table 2.** The best-fitting spectral parameters to the integrated EPIC pn spectrum. Flux<sup>o</sup> refers to the observed flux in the 0.1–10 keV energy band and Flux<sup>u</sup> refers to the unabsorbed, bolometric flux.

$N_H$	$4.2 \pm 0.1 \times 10^{21} \text{ cm}^{-2}$
$kT_{\text{bb}}$	$58.6^{+0.9}_{-1.2} \text{ eV}$
Line centre	$0.586 \pm 0.004 \text{ keV}$
EW	$257^{+23}_{-9} \text{ eV}$
Flux <sup>o</sup>	$1.35^{+0.05}_{-0.04} \times 10^{-12} \text{ erg s}^{-1} \text{ cm}^{-2}$
Flux <sup>u</sup>	$3.18^{+0.10}_{-0.16} \times 10^{-10} \text{ erg s}^{-1} \text{ cm}^{-2}$

data were taken within 3 months of each other, this phase offset is still valid despite the spin-up of the system.

## 5 SPECTRA

To fully utilize the data from the two observations (cf. Table 1), we combined the EPIC pn event files from the two epochs (we also did this for EPIC MOS2). We used single and double events for the pn spectrum, and single to quadruple events for the MOS spectrum and those events with FLAG = 0. We created response and auxiliary files using the *SAS* tasks *ARFGEN* and *RMFGEN*. The spectra are shown in Fig. 4. Ramsay et al. (2000) fitted X-ray spectra taken using *ROSAT* and *ASCA* using an absorbed blackbody model. We used *XSPEC* (Arnaud 1996) to fit the spectra, binned them so there was a minimum of 50 counts per bin and applied a low energy cut-off of 0.25 keV. The *XMM–Newton* spectra are not well fitted using such

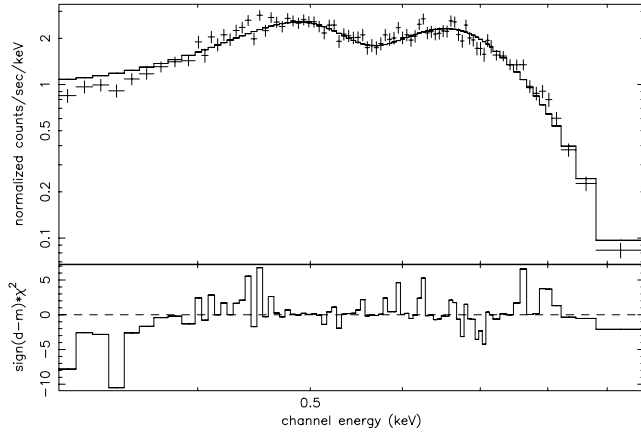


**Figure 4.** The integrated EPIC pn spectrum together with the best-fitting absorbed blackbody plus Gaussian line. We ignored events with energies below 0.3 and above 1 keV and binned the spectrum so that there was a minimum of 50 count bin<sup>-1</sup>.

a model. Various other models were fitted including: an absorbed two-temperature blackbody model; a thermal plasma model with varying element abundances; the previous model together with a blackbody; and an emission model together with a line in absorption around 0.55 keV. The only model that even approached a reasonable fit ( $\chi^2_{\nu} = 1.63$ , 79 d.o.f. in EPIC pn) was an absorbed blackbody plus broad Gaussian line in emission at 0.59 keV: this was an unexpected result (the fit to the EPIC MOS2 spectra was poorer giving  $\chi^2_{\nu} = 2.20$ , 29 d.o.f.: the response of the MOS cameras has changed over time, especially at energies  $<0.5$  keV). The spectral parameters for the integrated EPIC pn spectrum together with the flux is shown in Table 2. Spectra were also extracted from both RGS instruments: no distinct strong individual lines were detected with any confidence.

There are still significant residuals in the fit to the integrated spectrum using the absorbed blackbody plus line model. This is not unexpected because the softness ratio variation (Fig. 1) suggests that the shape of the spectrum changes over the bright X-ray phase. We therefore extracted four spectra covering the bright phase from the EPIC pn data. Again our model was an absorbed blackbody plus Gaussian line in emission near 0.59 keV. The spectral parameters for each spectrum were tied together apart from the normalizations, which were allowed to vary. A simultaneous fit to the four spectra gave  $\chi^2_{\nu} = 1.45$  (170 d.o.f.): the fit was not improved by letting the blackbody temperature vary. We find that the normalization of both the blackbody and line components roughly follow the shape of the X-ray light curve, although the normalization of the blackbody falls more rapidly compared with that of the Gaussian after intensity maximum resulting in a rise in the equivalent width (Fig. 5). Although the Gaussian line may not be physically realistic, it does, however, provide a suitable way of characterizing the spectra. To show the effect of the Gaussian line, we show in Fig. 6 the fits to phase resolved spectra including the line and then when we switch the line normalization to zero: the line has a very significant effect on the fits.

In light of these results, we revisited the *ROSAT* PSPC integrated spectrum and used the above model to fit that spectrum (extracted from the public archive in Rev2 calibrated form). We tied the normalization of the blackbody and Gaussian components so that they were the same ratio as found in the integrated *XMM-Newton* fits. We find that this model gives a better fit ( $\chi^2_{\nu} = 1.18$ , 6 d.o.f.) com-

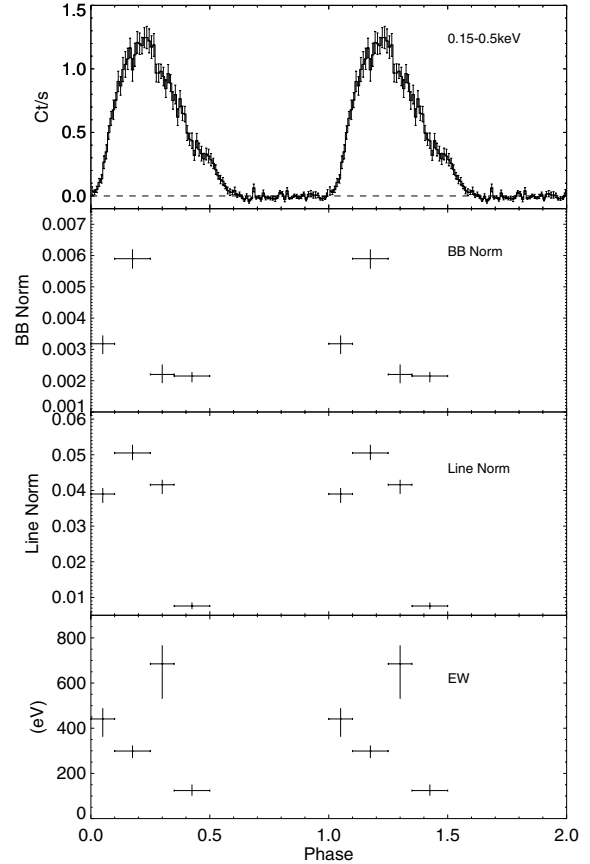


**Figure 5.** From the top: the 0.15–0.5 keV light curve folded on the 569 s and binned; the normalization of the blackbody component; the normalization of the Gaussian line included near 0.59 keV; the equivalent width of the Gaussian line.

pared to an absorbed blackbody ( $\chi^2_{\nu} = 1.58$ , 6 d.o.f.). We note that the resulting fit gives a lower absorption column ( $N_H = 1.7 \times 10^{21}$  cm<sup>-2</sup>) and higher blackbody temperature ( $kT_{bb} = 78$  eV) compared with the fits of Cropper et al. (1998). Ramsay & Cropper (2004) have noted that *ROSAT* observations of magnetic cataclysmic variable stars have shown a difference in the spectral parameters using Rev0 calibrated data and the Rev2 calibrated data.

## 6 DISCUSSION

We have presented observations of the X-ray source RX J1914+24 obtained using *XMM-Newton*. We have two main results: we find that RX J1914+24 is spinning up at a rate slightly greater than that determined by Strohmayer (2004a) and we find that the X-ray spectrum is very unusual showing a broad emission line at  $\sim 0.59$  keV in addition to the expected soft blackbody component.

### 6.1 The spin history of RX J1914+24

The models that have been used to explain the nature of RX J1914+24 and RX J0806+15 fall into two general categories: those involving accretion and those that do not. At face value, the results that show both RX J1914+24 and RX J0806+15 spinning up appear to rule out most of the accretion driven models: the double degenerate polar model (Cropper et al. 1998) and the direct impact model (Marsh & Steeghs 2002; Ramsay et al. 2002b). Unlike these

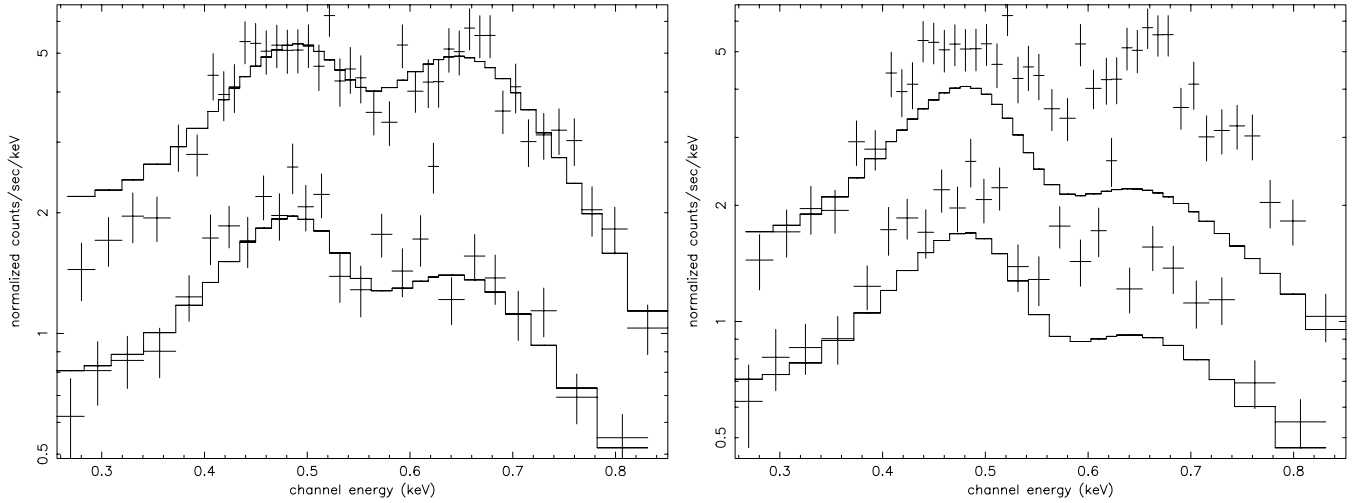


**Figure 6.** In the left-hand panel, we show two of the phase resolved EPIC pn spectra together with the best fit using an absorbed blackbody plus Gaussian line near 0.59 keV. In the right-hand panel, we emphasize the effect that the line has on the fit by setting its normalization to zero. In each panel, the upper spectrum covers  $\phi = 0.1\text{--}0.25$  and the lower spectrum  $\phi = 0.35\text{--}0.50$ . The spectra covering the other phase intervals have been omitted for clarity.

models, in which the observed intensity variation is attributed to the binary orbital period, Norton et al. (2004) attribute it to the spin period of an accreting white dwarf. No second period is detected because in this model the binary inclination is close to face-on.

The non-accreting model is the Unipolar-Inductor (UI) model proposed by Wu et al. (2002). In this model, a non-magnetic white dwarf traverses the magnetic field of the primary magnetic white dwarf, which causes large currents to be driven. Resistive dissipation occurs at the footpoints of the primary white dwarf and X-rays are released. This model also predicts that the system is an electron-cyclotron maser source in the UI phase (Willes, Wu & Kuncic 2004).

It is important to note that these systems have been observed for less than 10 yr and therefore the period decrease may simply be the result of a slow variation rather than a long-term trend.

In spite of the complicated interaction between the stellar spin rates and the binary orbital period, the change in the binary orbital period is determined only by the energy and angular momentum losses and redistribution in the system.

We illustrate this using the UI model given in Wu et al. (2002). For a binary with a secondary star in synchronous rotation with the orbit, it can be shown that the change in the orbital angular velocity  $\omega_o$  is given by

$$g(\omega_o) \left( \frac{\dot{\omega}_o}{\omega_o} \right) + \frac{2}{5} M_1 R_1^2 \omega_1 \dot{\omega}_1 = \dot{E}_{\text{gr}} + \dot{E}_{\text{diss}}, \quad (1)$$

where  $\dot{E}_{\text{gr}}$  is the energy loss as a result of gravitational radiation,  $\dot{E}_{\text{diss}}$  is the energy loss as a result of dissipation and  $\omega_1$  is the angular velocity of the primary (see Wu et al. 2002) for the explicit expression of  $g(\omega_o)$ .

In the UI model, the energy dissipation is caused by the resistive heating at the footpoints of the magnetic field lines on the magnetic white dwarf. In terms of the asynchronicity parameter of the spin of the primary,  $\alpha$  ( $\equiv \omega_1/\omega_o$ ), the energy dissipation is

$$\dot{E}_{\text{diss}} = -\frac{2}{5} \left| (1 - \alpha) M_1 R_1^2 \omega_o \dot{\omega}_1 \right|. \quad (2)$$

It can be shown that

$$\left( \frac{\dot{\omega}_o}{\omega_o} \right) = \frac{1}{g(\omega_o)} \left[ \dot{E}_{\text{gr}} + \frac{2}{5} \alpha M_1 R_1^2 \omega_o^2 \left( \frac{\dot{\omega}_1}{\omega_1} \right) \right]. \quad (3)$$

As  $(\dot{\omega}_1/\omega_1) = (\dot{\omega}_o/\omega_o) + (\dot{\alpha}/\alpha)$ , the rate of change in the orbital angular velocity may be expressed as

$$\left( \frac{\dot{\omega}_o}{\omega_o} \right) = \frac{\dot{E}_{\text{gr}}}{g(\omega_o)} \left[ 1 + \frac{2}{5} \frac{\alpha M_1 R_1^2 \omega_o^2}{\dot{E}_{\text{gr}}} \left( \frac{\dot{\alpha}}{\alpha} \right) \right] \left[ 1 - \frac{2}{5} \frac{\alpha M_1 R_1^2 \omega_o^2}{g(\omega_o)} \right]^{-1}. \quad (4)$$

This implies that the secular evolution of the orbital angular velocity is also determined by the coupling between the spin of the primary and the orbital rotation, in spite of the ultimate driver being the energy and angular momentum losses as a result of gravitational radiation. More detailed work is needed to determine the range of  $\alpha$  that could give rise to the observed spin-up rate.

## 6.2 X-ray luminosity

The lower panel of Fig. 3 shows that the observed count rate of RX J1914+24 varies by an order of magnitude. At the XMM–Newton epoch, the unabsorbed, bolometric flux determined using the model fits is shown in Table 2. As a result of projection effects, we correct the observed count rate by the ratio of the peak to mean count rate (a factor of 3.4), which gives a luminosity of  $\sim 1 \times 10^{35}$  erg s $^{-1}$  (for 1 kpc, Steeghs et al., in preparation). For the same distance this is  $\sim 2$  orders of magnitude lower than the X-ray luminosity estimate in Cropper et al. (1998): this a result of the higher absorption originally derived using the ROSAT PSPC spectrum. Fig. 3 implies that it has reached  $\sim 4 \times 10^{35}$  erg s $^{-1}$  in the past.

If the X-ray flux is driven by accretion and all of the accretion flow was liberated as X-rays, then the required mass transfer rate would exceed  $7 \times 10^{17}$  g s $^{-1}$  (or  $1.2 \times 10^{-8} M_{\odot}$  yr $^{-1}$ ). This would place it at the upper end of the range of mass transfer rates in known magnetic cataclysmic variables (Patterson 1994). However, the UI model proposed by Wu et al. (2002) is well within the constraints of the observed X-ray luminosity, despite its dependence on the orbital period of the system. Although the maximum power for a system with an orbital period of 569 s,  $M_2 = 0.1 M_{\odot}$  and a spin-orbit asynchronicity of 0.1 per cent is less than  $\sim 10^{34}$  erg s $^{-1}$  (Wu et al. 2002), an increase in the asynchronicity to 1.0 per cent would easily give rise to the observed luminosity.

Unless the dipole axis was closely aligned with the spin axis of the white dwarf, then this asynchronicity may be expected to have an observational signature. For an asynchronicity of 1 per cent, then that would give rise to a beat period of  $\sim 16$  h. The *XMM-Newton* X-ray observations are separated by 6 d and have relatively short durations so are not particularly suitable to search for such a period. A dedicated whole-Earth type of observing campaign is the best method to detect the signature of the asynchronous motion.

We note that an increase of the asynchronicity parameter would not significantly reduce the total lifetime of the binary, as the primary driver of the orbital evolution is gravitational radiation, in spite of short-term effects caused by spin-orbit coupling between the stars and the orbital rotation. An increase or decrease in  $\alpha$  would alter the duration of the duty cycle of the unipolar-induction process, and hence the brightness and discovery probability of the system.

### 6.3 The X-ray spectrum of RX J1914+24

The X-ray spectra of RX J1914+24 in Section 5 showed a soft blackbody component plus a broad feature resembling an emission line with a central energy close to  $\sim 0.59$  keV. We fitted the spectra with a range of possible models, including a two-temperature blackbody model and found that this did not give good fits. More detailed work is needed to determine if irradiated white dwarf atmosphere models can provide better fits (see Williams, King & Brooker 1987). Observations of the disc accreting double degenerate binaries, the AM CVn systems, show that their optical spectra can show metal abundances very different from solar (e.g. Marsh, Horne & Rosen 1991). The relative abundances are affected as a result of the CNO process and mixing in the common envelope phase of the binary. X-ray observations of AM CVn stars also show this non-solar abundance, e.g. Strohmayer (2004c), Ramsay et al., in preparation. Fits made using an emission model of different metal abundances for each element gave better fits than a two-temperature blackbody model, but poorer than a blackbody plus Gaussian line.

Using the blackbody plus Gaussian line, we find that the broad line is brightest at X-ray maximum, implying that it arises from a region close to the hotspot where most X-rays are emitted. The high-resolution RGS spectra, however, do not show any significant evidence for distinct individual lines. This is in contrast to *Chandra* observations of the 10.3-min binary ES Cet (Strohmayer 2004b), which shows tentative evidence for narrow emission lines at 0.47 and 0.89 keV. It is also in contrast to *XMM-Newton* observations of the double degenerate AM CVn system GP Com (Strohmayer 2004c), which show narrow emission lines of NVII, NVI, Ne X and Ne IX. The line centre of 0.59 keV is close to the O VII photoionized line at 0.57 keV, which has been detected in some intermediate polars (Mukai et al. 2003). The lines in these systems, however, have much narrower width.

It is possible that the broad feature could be line emission from material with large velocity dispersion. In the UI model, the large e.m.f. inside the magnetic flux tubes joining the two stars could accelerate charged particles, thus causing difficulty in the confinement of line emitting ionized atomic species right above the X-ray emitting hotspot. However, ionized particles could be present in a region close to the hotspot, yet outside the magnetic flux tubes that join the two stars (see the schematic illustration in Fig. 7). Nevertheless, we argue that the feature is unlikely to be the result of a low-order harmonic hump of cyclotron emission, as it would require a magnetic field strength  $\sim 10^{11}$  G in the emission region. Such a field is much stronger than the strongest magnetic fields measured in magnetic white dwarfs ( $\sim 10^{8-9}$  G, e.g. Barstow et al. 1995).

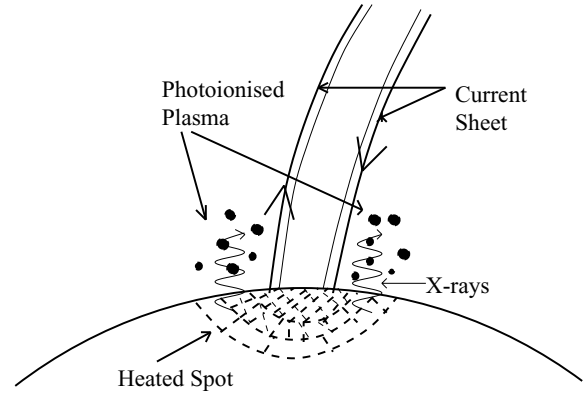


**Figure 7.** A schematic diagram showing one possible mechanism for producing the broad line seen near 0.6 keV. The line may be broadened as a result of the high velocities in the photoionized plasma.

### 6.4 The nature of RX J1914+24

The true nature of RX J1914+24 is still unclear. Whilst the UI model of Wu et al. (2002) perhaps comes closest to predicting the observed characteristics, it too has question marks. For instance, Barros et al. (2005) explored the set of binary parameters (masses, binary inclination and the spin-magnetic axis offset) that could give rise to the observed X-ray light curves of both RX J1914+24 and RX J0806+15 and concluded that only a very small set of parameter space could work. This implies that either the UI model is unlikely to be applicable to these systems or that the magnetic white dwarf has a field structure more complex than a simple dipole.

The *XMM-Newton* data presented here raise a number of issues, all of which need further work to address them in detail.

(i) RX J1914+24 has a highly unusual X-ray spectrum, with a peculiar feature near 0.6 keV. Grating spectra with higher signal-to-noise ratios are required and more theoretical work is needed to determine if the UI model can produce such an X-ray spectrum.

(ii) We need to determine how system parameters, such as the asynchronicity parameter  $\alpha$ , can produce the observed spin-up rate and X-ray luminosity.

(iii) Unless the spin and magnetic axes are very closely aligned, the asynchronicity should give rise to a beat period. More work is needed observationally to search for such a period and theoretically to predict the amplitude of such a beat period.

(iv) Steeghs et al., in preparation, show an optical spectrum that has features similar to that of a K star. To resolve the nature of these features, phase resolved spectroscopy is urgently required. If RX J1914+24 is a triple system, then this will obviously have implications for the evolutionary history of the systems.

### ACKNOWLEDGMENTS

We thank Andrew Willes for useful discussions and the anonymous referee for useful suggestions that clarified aspects of the text. This is work based on observations obtained with *XMM-Newton*, an ESA science mission with instruments and contributions directly funded by ESA Member States and the USA (NASA). These observations were part of the *XMM-Newton* OM guaranteed time programme.

### REFERENCES

- Arnaud K. A., 1996, in Jacoby G., Barnes J., eds, ASP Conf. Ser. Vol. 101, Astronomical Data Analysis Software and Systems V. Astron. Soc. Pac., San Francisco, p. 17

- Barros S. C. C., Marsh T. M., Groot P., Nelemans G., Ramsay G., Roelofs G., Steeghs D., Wilms J., 2005, MNRAS, in press (doi: 10.1111/j.1365-2966.2005.08740.x)
- Barstow M. A., Jordan S., O’Donoghue D., Burleigh M. R., Napiwotzki R., Harrop-Allin M. K., 1995, MNRAS, 277, 971
- Cropper M., Harrop-Allin M. K., Mason K. O., Mittaz J. P. D., Potter S. B., Ramsay G., 1998, MNRAS, 293, L57
- Cropper M., Haberl F., Zane S., Zavlin V. E., 2004, MNRAS, 351, 1099
- Hakala P., Ramsay G., Wu K., Hjalmarsdotter L., Järvinen S., Järvinen A., Cropper M., 2003, MNRAS, 343, L10
- Hakala P., Ramsay G., Byckling K., 2004, MNRAS, 353, 435
- den Herder J. W. et al., 2001, A&A, 365, L7
- Israel et al., 2002, A&A, 386, L13
- Israel et al., 2003, ApJ, 598, 492
- Marsh T. R., Steeghs D., 2002, MNRAS, 331, L7
- Marsh T. R., Horne K., Rosen S., 1991, ApJ, 366, 535
- Mukai K., 1993, Legacy, 3, 21
- Mukai K., Kinkhabwala A., Peterson J. R., Kahn S. M., Paerels F., 2003, ApJ, 586, L77
- Norton A. J., Haswell C., Wynn G. A., 2004, A&A, 419, 1025
- Patterson J., 1994, PASP, 106, 209
- Ramsay G., Cropper M., 2004, MNRAS, 347, 497
- Ramsay G., Cropper M., Wu K., Mason K. O., Hakala P., 2000, MNRAS, 311, 75
- Ramsay G., Hakala P., Cropper M., 2002a, MNRAS, 332, L7
- Ramsay G., Wu K., Cropper M., Schmidt G., Sekiguchi K., Iwamuro F., Maihara T., 2002b, MNRAS, 333, 575
- Strohmayer T. E., 2002, ApJ, 581, 577
- Strohmayer T. E., 2003, ApJ, 593, L39
- Strohmayer T. E., 2004a, ApJ, 610, 416
- Strohmayer T. E., 2004b, ApJ, 614, L121
- Strohmayer T. E., 2004c, ApJ, 608, L53
- Strüder L. et al., 2001, A&A, 365, L18
- Turner M. et al., 2001, A&A, 365, L27
- Warner B., Woudt P., 2002, PASP, 792, 129
- Willes A. J., Wu K., Kuncic Z., 2004, PASA, 21, 248
- Williams G. A., King A. R., Brooker J. R. E., 1987, MNRAS, 266, 725
- Woudt P., Warner B., 2003, in Sion E., Vennes S., Shipman H., eds, Proc. IAU JD5, White Dwarfs: Galactic and Cosmological Probes (astro-ph/0310494)
- Wu K., Cropper M., Ramsay G., Sekiguchi K., 2002, MNRAS, 331, 221

This paper has been typeset from a  $\text{\TeX}/\text{\LaTeX}$  file prepared by the author.